

UCLA

UCLA Previously Published Works

Title

Maintenance of CD4 T cell fitness through regulation of Foxo1

Permalink

<https://escholarship.org/uc/item/9pd3v30v>

Journal

Nature Immunology, 19(8)

ISSN

1529-2908

Authors

Newton, Ryan H
Shrestha, Sharad
Sullivan, Jenna M
et al.

Publication Date

2018-08-01

DOI

10.1038/s41590-018-0157-4

Peer reviewed



Published in final edited form as:

Nat Immunol. 2018 August ; 19(8): 838–848. doi:10.1038/s41590-018-0157-4.

Maintenance of CD4 T cell fitness through regulation of Foxo1

Ryan H. Newton^{1,10}, Sharad Shrestha², Jenna M. Sullivan³, Kathleen B. Yates^{4,5}, Ewoud B. Compeer⁶, Noga Ron-Harel⁷, Bruce R. Blazar⁸, Steven J. Bensing⁹, W. Nicholas Haining^{4,5}, Michael L. Dustin⁵, Daniel J. Campbell³, Hongbo Chi², and Laurence A. Turka^{1,11,*}

¹Center for Transplantation Sciences, Department of Surgery, Massachusetts General Hospital and Harvard Medical School, Boston, MA, USA.

²Department of Immunology, St Jude Children's Research Hospital, Memphis, TN, USA.

³Department of Immunology, University of Washington, Seattle and Immunology Program, Benaroya Research Institute, Seattle, WA, USA.

⁴Division of Pediatric Hematology and Oncology, Children's Hospital, Boston, MA, USA.

⁵Broad Institute of Harvard and Massachusetts Institute of Technology, Cambridge, MA, USA.

⁶Kennedy Institute of Rheumatology, Nuffield Department of Orthopedics, Rheumatology and Musculoskeletal Sciences, University of Oxford, Oxford, UK.

⁷Department of Cell Biology, Harvard Medical School, Boston, MA, USA.

⁸Department of Pediatrics, Division of Blood and Marrow Transplantation, University of Minnesota, Minneapolis, MN, USA.

⁹Department of Molecular and Medical Pharmacology, University of California, Los Angeles, Los Angeles, CA, USA.

¹⁰Present address: Celsius Therapeutics, Cambridge, MA, USA.

¹¹Present address: Rheos Medicines, Cambridge, MA, USA.

Abstract

Foxo transcription factors play an essential role in regulating specialized lymphocyte functions and in maintaining T cell quiescence. Here, we used a system in which Foxo1 transcription-factor activity, which is normally terminated upon cell activation, cannot be silenced, and we show that

Reprints and permissions information is available at www.nature.com/reprints.

***Correspondence and requests for materials** should be addressed to L.A.T., lturka@rheosrx.com.

Author contributions

R.H.N. and L.A.T. designed the study, interpreted data and wrote the manuscript. R.H.N. performed experiments. S.S. performed experiments with Rictor flox/flox animals. J.M.S. performed experiments to help characterize autoimmunity in CD4^{Cre} Foxo1^{AAA/+} animals. K.B.Y. assisted with RNA-seq data analysis. E.B.C. performed immunological synapse imaging experiments. N.R.-H., B.R.B., S.J.B., W.N.H., M.L.D., D.J.C. and H.C. assisted with data analysis and interpretation.

Competing interests

The authors declare no competing interests.

Additional information

Supplementary information is available for this paper at <https://doi.org/10.1038/s41590-018-0157-4>.

Publisher's note: Springer Nature remains neutral with regard to jurisdictional claims in published maps and institutional affiliations.

enforcing Foxo1 activity disrupts homeostasis of CD4 conventional and regulatory T cells. Despite limiting cell metabolism, continued Foxo1 activity is associated with increased activation of the kinase Akt and a cell-intrinsic proliferative advantage; however, survival and cell division are decreased in a competitive setting or growth-factor-limiting conditions. Via control of expression of the transcription factor Myc and the IL-2 receptor β -chain, termination of Foxo1 signaling couples the increase in cellular cholesterol to biomass accumulation after activation, thereby facilitating immunological synapse formation and mTORC1 activity. These data reveal that Foxo1 regulates the integration of metabolic and mitogenic signals essential for T cell competitive fitness and the coordination of cell growth with cell division.

Phosphatidylinositol 3-kinases (PI3Ks) are central integrators of signal transduction, coupling cell-surface receptors to intracellular signaling pathways, such as the Akt and mTOR pathways, to regulate growth and metabolism¹. Key activators of the PI3K pathway in T cells, such as the IL-2 receptor, play a critical role in enabling cells to exit quiescence and progress through the cell cycle^{2,3}. Among the primary targets of the PI3K–Akt pathway in T cells are transcription factors from the Foxo family. Both Foxo1 and Foxo3 have largely redundant but complex roles in maintaining T cell quiescence and controlling the response to growth factors and inflammatory stress^{4,5}. In quiescent cells, Foxos are restricted to the nucleus and maintain transcriptional activity; cell activation induces the Akt-mediated phosphorylation of three evolutionarily conserved serine and threonine residues on Foxos, thus leading to Foxo exclusion from the nucleus and hence termination of transcriptional activity. Loss of Foxo1 in T cells results in the development of a mild lymphoproliferative and autoimmune phenotype^{6,7}. This phenotype is distinct from that in mice with regulatory T cell (T_{reg})-specific deletion of Foxo1, in which lethal inflammation is observed after loss of dominant tolerance without compromised conventional T cell function⁸.

The kinase mTOR coordinates metabolic pathways that dictate T cell fate, although the mechanisms underlying this role have not been completely described. T_{reg} cells from mice with a T_{reg} -specific deletion of Raptor, an essential component for mTOR complex 1 activity, are deficient in cholesterol and lipid metabolism, and consequently these cells exhibit proliferation and maintenance defects⁹. In mice with Raptor deletion in all T cells, glycolytic, lipid-synthesis and oxidative-phosphorylation programs are severely impaired, thus preventing T cell exit from quiescence¹⁰. These differences reflect altered use of metabolism in T cells of different lineages and indicate that mTOR is central in driving each of these programs.

How the activity of Foxos intersects with these signaling pathways is incompletely understood, as is the role that termination of Foxo1 activity plays in coordinating the T cell response to stimulation. To understand how control of Foxo1 transcriptional activity regulates T cell function and homeostasis, we used mice that conditionally express a constitutively active Foxo1 protein (Foxo1^{AAA}). We show that inactivation of Foxo1 is required to maintain CD4 T cell and T_{reg} cell homeostasis in vivo, because T cell-specific Foxo1^{AAA} expression provokes severe autoimmunity in mice, which is preventable with wild-type cells. Using CD4 T cells inducibly expressing Foxo1^{AAA}, we show that maintaining Foxo1 activity leads to a decrease in cell size and cholesterol accumulation, and

an inability to sustain signaling by the nutrient sensor mTORC1, but paradoxically also increases cell-division rates. Further analysis indicated that this phenotype was caused by loss of expression of the IL-2R β -chain and STAT5-dependent upregulation of the transcription factor *Myc*. Together, these data show that termination of Foxo1 activity is required to coordinate cell growth with cell proliferation, a critical process needed to maintain both homeostasis and responses to stimulation.

Results

Inactivation of Foxo1 is required to maintain CD4 T cell and T_{reg} cell homeostasis.

To study how the maintenance of Foxo1 transcriptional activity affects T cell homeostasis and activation, we used mice expressing a transgene, controlled by Cre recombinase expression, in which the three Akt-targeted residues are mutated to alanines (Rosa26-flox-STOP-FOXO1^{AAA}-IRES-GFP; Foxo1^{AAA}). Mice with CD4^{Cre}-mediated expression of one allele of Foxo1^{AAA} (CD4^{Cre} Foxo1^{AAA/+}) developed a severely moribund state as early as 4 weeks of age, showing stunted growth and ulcerative dermatitis (Fig. 1a) associated with a prominent mononuclear cell infiltrate in the liver and lungs, splenomegaly and lymphadenopathy (Fig. 1a and Supplementary Fig. 1a,b). In the transgenic mice, compared with wild-type mice, despite increased cellularity of the spleen and lymph nodes, a selective decrease in both the frequency and number of CD4 T cells was observed, but there were no significant differences in CD8 T cell numbers (Fig. 1b). T_{reg} cell frequencies were severely decreased, and within the remaining T_{reg} cell population, CD25 expression was downregulated despite high expression of the suppressive molecules ICOS and CTLA-4 (Fig. 1c and Supplementary Fig. 1c–e).

Both CD4 and CD8 T cells exhibited an activated phenotype with elevated expression of CD44 and Ki-67, and produced high amounts of the cytokine IFN- γ and the serine protease granzyme B, respectively, directly ex vivo (Supplementary Fig. 1f–h and data not shown). An expanded and activated B cell population developed concomitantly with an elevated frequency of Tfh cells and of IL-4-producing cells within the remaining CD4 population (Supplementary Fig. 2a–e). We observed elevated serum IgM, IgG and particularly IgG1 antibodies, as well as IgM and IgG autoantibodies reactive toward HEP-2 cells (Supplementary Fig. 2f–j). This result was associated with renal IgG deposition resembling lupus nephritis, as well as anemia and hypoglycemia (Supplementary Fig. 2k–m).

To determine whether the observed alterations in CD4 T cells and T cells were cell intrinsic with respect to Foxo1^{AAA} expression, we generated bone marrow chimeras. *Rag1*^{-/-} recipient mice receiving bone marrow from Foxo1^{AAA} donors (single chimeras) reproduced the cellular phenotype of nonchimeric CD4^{Cre} Foxo1^{AAA/+} mice (showing a paucity of CD4 T cells and T_{reg} cells, and a high proportion of activated T cells), with immune cell infiltrates in visceral organs and skin, and six of eight mice exhibited a failure to thrive by 16 weeks post-transfer (Fig. 1d). In contrast, autoimmunity was not observed in mixed bone marrow chimeras. Foxo1^{AAA} T cells from the mixed chimeras maintained a quiescent state (CD44^{lo}CD62L^{hi} and PD-1^{neg}) (Fig. 1e and data not shown), thus suggesting that cells derived from wild-type bone marrow provided dominant tolerance, blocking activation of Foxo1^{AAA} T cells and thereby preventing disease. A disproportionate percentage of both

conventional CD4⁺ T cells and T_{reg} cells were derived from wild-type bone marrow, whereas both wild-type and Foxo1^{AAA} hematopoietic stem cells contributed equally to the reconstituted CD8 T cell compartment (Fig. 1f,g). Together, these results demonstrate that inactivation of Foxo1 is required for cell-intrinsic maintenance of both conventional CD4⁺ T cells and T_{reg} cells.

Foxo1 activity suppresses the coordination of CD4 T cell growth and proliferative pathways.

The absence of autoimmunity in the mixed bone marrow chimeras allowed us to determine how maintained Foxo1 activity affected T cell transcriptional profiles without the potential bias of background inflammation (Supplementary Fig. 3a,b). We found few notable differences in gene expression between wild-type and Foxo1^{AAA}-expressing CD4 peripheral T cells, thus reinforcing our observation that Foxo1^{AAA} expression does not intrinsically affect CD4 T cell quiescence (Fig. 1h). To understand how dysregulation of Foxo1 affected activated CD4 T cells in vivo, we took advantage of the observation that the absence of a functional T_{reg} cell population in single chimeric recipients of Foxo1^{AAA} bone marrow led to spontaneous CD4 T cell activation, and we therefore compared these cells and Foxo1^{AAA}-expressing CD4 T cells from mixed bone marrow chimeras (Fig. 1i). We observed that the Foxo1^{AAA} CD4 T cells from single-chimeric mice exhibited hallmarks of T cell activation and upregulated expression of multiple chemokine and cytokine receptors and ligands (Supplementary Fig. 3c–e). Gene-set enrichment analysis of differentially expressed genes in Foxo1^{AAA} CD4 T cells from single-chimeric mice indicated that additional pathways, including ribosome biogenesis and the Myc transcription factor, which are largely interdependent, as well as cholesterol biosynthesis, were unexpectedly downregulated as compared with levels in the quiescent Foxo1^{AAA} population (Fig. 1j,k).

The unexpected finding of downregulation of Myc, cholesterol biosynthesis and ribosome biogenesis pathways in activated versus resting Foxo1^{AAA} CD4 T cells led us to ask how this result might compare with those in activated versus resting wild-type CD4 T cells. To answer this question, we made use of public data comparing conventional CD4 T cells from wild-type mice and conventional CD4 T cells from Scurfy mice¹¹. This comparator group seemed particularly apt, given that conventional CD4 T cell activation arises in conjunction with defects in the T_{reg} cell compartment in both Scurfy mice and our single-chimeric mice. Gene ontology analysis revealed that genes involved in cell-cycle progression and cell division, and in cytokine signaling, were upregulated in conventional CD4 T cells from Scurfy mice and were not comparably induced in Foxo1^{AAA} CD4 T cells from single-chimeric mice (Supplementary Fig. 4a,b). In addition, ribosome-biogenesis and cholesterol-biosynthesis pathways were not comparably downregulated in effector T cells from Scurfy mice, thus indicating that dysregulation of these pathways was not merely a consequence of the loss of a regulatory population (Supplementary Fig. 4c,d). Given the importance of Foxo proteins in controlling metabolism^{12–14}, we reasoned that these differences might be a consequence of failed metabolic checkpoints coupled to cell-cycle progression. Indeed, we found that many genes involved in metabolic pathways previously shown to be upregulated in wild-type T cells after activation were suppressed in activated Foxo1^{AAA} CD4 T cells (compared with quiescent AAA CD4 T cells; Supplementary Fig. 5)^{15,16}.

To further explore the consequences of Foxo1^{AAA} expression in CD4 T cells in a noninflammatory environment, we bred Foxo1^{AAA} mice to CD4^{Cre-ERT2} mice to allow for acute induction of Foxo1^{AAA} in peripheral CD4 T cells after administration of tamoxifen. Mice were given tamoxifen for 5 d, and organs were harvested on day 8. In cultures of whole splenocytes stimulated with anti-CD3 plus anti-CD28 (anti-CD3/28), we observed less proliferation in Foxo1^{AAA}-expressing cells (GFP⁺) than in cells from the same animal in which Foxo1^{AAA} was not induced by tamoxifen (GFP⁻) (Fig. 2a). This proliferation defect was reversed, and in fact a hyperproliferative phenotype was revealed, when GFP⁺ and GFP⁻ cells were sorted before activation and maintained separately as isolated cultures (isocultures; Fig. 2b). A hypoproliferative phenotype was once again observed when GFP⁺ and GFP⁻ cells were recombined and cocultured after sorting (Fig. 2c), thus confirming a cell-intrinsic proliferative advantage of Foxo1^{AAA} T cells in isolation, yet a competitive disadvantage in the presence of wild-type competitors.

Despite the hyperproliferative phenotype demonstrated in iso-cultures, GFP⁺ cells had a greatly diminished cell size (Fig. 2d). This decrease was seen throughout ‘generations’ (i.e., cell divisions), thus indicating that this observation was not a consequence of a greater proportion of cells having gone through a higher number of divisions. This decrease in cell size was also seen in cocultures (data not shown), and thus this trait was not linked to proliferative capacity. In vivo, when the proportion of GFP⁺ cells compared with that of YFP⁺ cells from control CD4^{Cre-ERT2} Rosa26^{YFP/+} mice was measured in the blood over time, we observed decreased maintenance of Foxo1^{AAA}-expressing cells after tamoxifen treatment (Fig. 2e), and this observation was also accompanied by decreased cell size among dividing cells (Fig. 2f). These findings indicate that the competitive disadvantage observed for Foxo1^{AAA}-expressing cells in vitro is present in vivo as well.

Foxo1 activity limits cell metabolism via impaired Myc and IL-2 signaling.

During the first 2 d of activation (i.e., before proliferative differences were observed), standard outputs of metabolic activation, including consumption of glucose and glutamine, and production of lactate and glutamate, were not affected by Foxo1^{AAA} expression (Fig. 3a–d and Supplementary Fig. 6a). However, these outputs were significantly decreased by day 3 (Fig. 3a–d), thus prompting us to examine T cell metabolism through bioenergetic analysis at that time point. As assessed by the extracellular acidification rate (ECAR) and oxygen consumption rate (OCR), we found that both basal and maximal glycolytic and oxidative rates were greatly diminished at day 3, thus indicating that cell metabolism is constrained by constitutive Foxo1 activity (Fig. 3e–k). We measured expression of key metabolic regulators and found that although expression of the transcription factor Hif-1 α was higher than that in wild type, in agreement with a high ECAR/OCR ratio, the normal pattern of Myc expression was disrupted (Fig. 3l). Specifically, Myc induction at 24 h was not affected, but at later time points, Myc expression was lower in Foxo1^{AAA}-expressing cells (Supplementary Fig. 6b). This result was independent of proliferative state, because it was observed in both the iso- and cocultures and was associated with low levels of *Myc* mRNA (Fig. 3m and Supplementary Fig. 6c,d).

IL-2 signals contribute to Myc upregulation after T cell activation^{17,18}. Furthermore, sustained IL-2 signals are critical to maintain Myc expression postactivation, whereas blockade of IL-2 signals with inhibitors of JAK kinases, or by IL-2 withdrawal, results in a rapid decrease in Myc expression. Although we found no alterations in IL-2 mRNA or protein production, or in the expression of the α or γ_c chain of IL-2R (CD25 and CD132, respectively; data not shown), we observed that expression of the IL-2R β chain (CD122) was lower at baseline than that in wild-type cells, and it became progressively and selectively downregulated after activation (Fig. 4a–c). However, we could not attribute the lower expression of CD122 to the failure to sustain Myc, because CD122 expression was lower than that in wild type at day 0 (i.e., before the normal induction of Myc) and became progressively lower even before the defect in Myc expression was seen. Furthermore, we observed a decrease in neither CD122 transcripts, as measured by qPCR, nor total protein levels, as assessed by both immunoblotting and intracellular staining followed by flow cytometry (Supplementary Fig. 6e–g), thus indicating that only surface expression was decreased.

The diminished expression of CD122 correlated with decreased activation of the transcription factor STAT5 (phosphorylated (p-) STAT5) after stimulation (Fig. 4d). In agreement with this result, stimulation of cells with additional IL-2 during the first 24 h of activation did not restore p-STAT5 in GFP⁺ cells (data not shown). Furthermore, GFP⁺ cells were selectively sensitive to inhibition of growth signals by anti-IL-2, as indicated by enhanced cell death, thus suggesting that the observed competitive disadvantage in the coculture system might be conferred by compromised IL-2 signaling (Fig. 4e).

In activated T cells, increased glycolysis and mitochondrial metabolism provide precursors for biosynthetic pathways, thereby linking Myc-dependent catabolism with anabolic generation of complex molecules^{10,16,19,20}. Given the observed defect in cell growth, we examined pathways that contribute to biomass accumulation. In agreement with our transcriptome analysis indicating dysregulation of genes involved in cellular cholesterol metabolism (Fig. 1j,k), we observed a notable decrease in the free-cholesterol levels of Foxo1^{AAA}-expressing cells compared with wild-type T cells, as assessed by Filipin staining. This result was observed as early as 24 h postactivation and increased by 48 h in culture (Fig. 5a,b). We measured transcript levels of genes involved in cholesterol biosynthesis during initial stages of T cell activation, including those that were significantly altered on the basis of gene expression profiling of chimeric mice, and we found no observable defects, thus suggesting that Foxo1 activity does not directly regulate this gene program and that decreased cholesterol accumulation is linked to the observed defects in catabolic pathways (data not shown). Microscopy images showing GFP⁻ and GFP⁺ cells with a markedly different degree of Filipin staining further suggested that the decrease in cellular cholesterol was not merely due to decreased biomass (Fig. 5b).

To determine the role of decreased Myc and IL-2 signaling in the suppression of both cholesterol accumulation and cell size in Foxo1^{AAA}-expressing cells, we used a retroviral system to restore these pathways. Delivery of a constitutively active STAT5b construct increased expression of Myc, normalized the cholesterol deficit in GFP⁺ cells and further increased the cholesterol content of GFP⁻ cells (Fig. 5c–e). This result not only confirms

that IL-2 signals upregulate Myc but also indicates that IL-2 regulates cellular cholesterol levels. Furthermore, rather than occurring via a direct translational or transcriptional effect, Foxo1-mediated repression of STAT5 activity accounts for loss of Myc, and CD122 is a key intermediary between Foxo1 and Myc. In contrast, retroviral overexpression of Myc was sufficient to rescue the defect in cell size in Foxo1^{AAA}-expressing cells but had no effect on cholesterol accumulation. Together, these results indicate that Foxo1 activity uncouples cholesterol accumulation and overall biomass accumulation via a Myc-independent mechanism (Fig. 5f–h).

Cholesterol-dependent immunological synapse formation is controlled by Foxo1 signals.

Cholesterol is crucial for the formation of an immunological synapse^{21,22}. To examine how dysregulation of metabolism after activation of Foxo1^{AAA}-expressing cells affects their ability to form an immunological synapse, we used total internal reflection fluorescence microscopy on cells that were preactivated for 3 d and then allowed to interact with supported lipid bilayer (SLB)-containing fluorescent ICAM-1 and CD80, and anti-CD3e stimulatory antibody 2C11. We found that Foxo1^{AAA}-expressing cells did not develop a mature synapse with a central supramolecular activation cluster (cSMAC), as defined by the appearance of a highly dense 2C11 area excluding ICAM-1 at the site of the SLB interaction (Fig. 6a–e). Additionally, we visualized the SLB-bound T cell surface area by using interference reflection microscopy, and we found that this area was greatly reduced in Foxo1^{AAA}-expressing cells, in agreement with their diminished cholesterol content (Fig. 6a,f). To determine whether these features were a direct consequence of diminished cholesterol content, we supplemented cells with water-soluble cholesterol immediately before imaging. This supplementation restored synapse formation, recruitment of T cell receptor (TCR) and the integrin LFA-1, and T cell spreading to levels equal to or above those seen in control cells (Fig. 6a–f). This result suggests that downstream signaling effects may potentially emanate from a defect in cholesterol-dependent immunological synapse formation.

Maintained Foxo1 activity dysregulates Akt and impairs lysosomal biogenesis and mTORC1 signaling.

Because cSMAC formation is associated with termination of TCR signaling by shedding of TCR molecules in extracellular vesicles²³, and given the role of Foxos in T cell metabolism, the defective cSMAC formation in Foxo1^{AAA} T cells prompted us to investigate TCR-coupled Akt activation. In contrast to reduced cellular metabolism, we observed enhanced activation (i.e., phosphorylation) of Akt (Fig. 7a,b). Similarly to Akt, Sgk1 has been shown to phosphorylate the three conserved serine/threonine residues on Foxos that also are targeted by Akt²⁴. We noted an increase in phosphorylation of the Sgk1 target Ndr1, thus indicating that Sgk1 activity was also elevated and suggesting that Foxos participate in a self-regulatory feedback mechanism to limit their activity (Fig. 7a). However, this increase in p-Akt did not translate into an increase in mTORC1 activity (as assessed by p-mTOR, p-S6 and p-4E-BP1 levels; Fig. 7a), nor was it reflected by increased mTORC2 activity (as assessed by p-PKC α levels) (Supplementary Fig. 7a). Instead we observed decreases in both mTORC1 and mTORC2 activity, in agreement with cell growth defects and diminished Myc protein levels. We explored the possibility that decreased mTORC1 activity, or Foxo1

activity itself, might result in a hyperautophagic state potentially contributing to cell-growth defects. However, we found that regulation of autophagy, as assessed by LC3-I/II immunoblotting, remained intact (data not shown).

We similarly observed elevated Akt phosphorylated on Thr308 (Supplementary Fig. 7b). This event is mediated by Pdk1 (ref. ¹); however, Pdk1 activity was not elevated, nor did we observe an increase in expression of the mTORC2 component Rictor to account for increased Ser473 phosphorylation (Supplementary Fig. 7c and data not shown). Additionally, we tested a role for the kinase DNA-PK, which has previously been shown to target Akt on Ser473 (ref. ²⁵) and found that whereas an inhibitor of DNA-PK reduced Ser473 phosphorylation in wild-type cells, thus indicating that this kinase does contribute to activation of Akt after T cell activation, Foxo1^{AAA} T cells maintained dramatically high Ser473 phosphorylation, thus indicating that DNA-PK activity does not appear to be dysregulated or critical for the observed hyperactivation of Akt (Supplementary Fig. 7d). However, we did observe that, unlike wild-type cells, Foxo1^{AAA}-expressing cells maintained surface CD3 levels after activation and did not upregulate PD-1 expression, thus potentially accounting for increased signaling through the T cell receptor²⁶, failure to recruit phosphatases to TCR signaling complexes or an inability to terminate TCR signaling via vesicle release²⁷ (Supplementary Fig. 7e,f). Additionally, we observed a dramatic decrease in the expression of the tumor suppressor PTEN, which plays a dominant role in negatively regulating PI3K signals (Supplementary Fig. 7g). Together, these data suggest that multiple mechanisms are likely to increase activation of Akt.

To further probe the role of Akt activation downstream of Foxo1 in the cellular phenotype of AAA mice, we bred CD4^{Cre} Foxo1^{AAA} mice to Rictor^{fl/fl} mice. We found that loss of Rictor did not reverse the abnormal lymphoid composition of CD4^{Cre} Foxo1^{AAA} mice (Fig. 7c,d), nor did it prevent the increase in Akt activation in Foxo1^{AAA} CD4 T cells after stimulation (Fig. 7e). These findings suggest that mTORC2 is not required for activation of Akt in the context of constitutive Foxo1 activity.

mTORC1 activation depends on both growth factors (via Akt) and nutrients (in particular, amino acids), and takes place specifically at the lysosome^{15,28}. Although activation of Akt is necessary for mTORC1 activity in most contexts, it is not sufficient, and lysosomal cholesterol has recently been identified as a key 'nutrient' required for mTORC1 recruitment and activation at the lysosomal surface²⁹. Given the decrease in membrane cholesterol levels, we reasoned that lysosomal content might also be decreased, because pathways that control accumulation of both lysosomes and cholesterol overlap in their regulation and could both potentially alter activation of mTORC1 (refs. ^{29,30}). Indeed, we observed decreased maturation of the lysosomal-membrane protein Lamp-1 in Foxo1^{AAA}-expressing cells, as assessed by detection of its glycosylated form by SDS-PAGE, thus suggesting a defect in cholesterol-dependent lysosomal biogenesis (Fig. 8a). This finding led us to reexamine the loss of CD122 surface expression that we previously could not account for. We hypothesized that shuttling and/or recycling of CD122 via the endocytic or lysosomal pathway might be defective. By blocking endocytosis with Dynasore (a chemical inhibitor of dynamin- and clathrin-mediated endocytosis), we restored surface CD122 levels in a dose-dependent

manner (Fig. 8b). This result confirms that a defect in this pathway accounts for decreased surface expression of CD122.

Further evidence of abnormal mTOR activity was obtained through confocal microscopy. In the absence of growth factors and nutrients, wild-type cells showed diffuse mTOR staining without Lamp-1 colocalization (Supplementary Fig. 8). When nutrients were supplemented to the medium, mTOR staining became punctate and colocalized with the lysosome. In contrast, in Foxo1^{AAA}-expressing cells, we observed constitutive colocalization of mTOR with Lamp-1, but most notably, a greatly diminished Lamp-1 signal. Importantly, this phenotype persisted even when Foxo1^{AAA}-expressing cells were activated (Fig. 8c). These data suggest that Foxo1 enforces physiological constraints on cholesterol and lysosomal content such that mTORC1 activity cannot be sustained, despite elevated levels of Akt activation. Thus, the effect of maintaining Foxo1 activity results in a benefit/cost ratio that may support a proliferative advantage under specific settings but ultimately compromises metabolic fitness and the ability of these cells to persist, either under homeostatic conditions or in a competitive environment.

Discussion

Previous work has linked silencing of Foxo1 to enabling Myc-dependent metabolic activity and growth in endothelial cells¹⁴. Our studies confirm and extend this concept yet also indicate a number of crucial new findings. In contrast to the role of Foxo1 in promoting endothelial cell quiescence, we did not observe a coordinated decrease in the proliferative and metabolic activities of CD4 T cells by maintaining Foxo1 activity. Instead, we found that inactivation of Foxo1 is, in fact, needed to match proliferative and metabolic rates.

In response to growth-factor withdrawal, CD4 T cells reduce cell surface area to minimize energy expenditure while conserving bio-mass³¹. Under such conditions of nutrient stress, regulation of cell size can be thought of as a means to promote survival. Our data indicate a key role of Foxo1 in the process. In the context of maintained Foxo1 activity, we found a cell-intrinsic decrease in cell size and cholesterol content independent of nutrient availability and increased viability after activation despite diminished growth-factor signals. Moreover, these events are partly dependent on repression of Myc.

In addition to the diminished expression of Myc seen with continued Foxo1 activity, we observed decreases in mTORC1 and mTORC2 signaling. mTORC1 is activated and sustained by both glutaminolysis³² and glycolysis³³, pathways that are driven by Myc in activated T cells^{16,34}; moreover, mTORC1 activity itself can regulate Myc translation³⁵. Our data show that although increasing Myc expression via retroviral delivery rescues cell-growth defects, only restoration of signals downstream of IL-2 enables the accumulation of cholesterol that under normal circumstances supports cell growth. Thus, Foxo1 controls both Myc-dependent and Myc-independent growth pathways that diverge at the level of IL-2 signaling.

A specific defect in cholesterol synthesis has been demonstrated in T_{reg} cells that lack mTORC1 activity, owing to a loss of Raptor⁹. Although mTORC1 signaling is diminished

by Foxo1 activity, our data suggest that this effect is, at least in part, a consequence of a cholesterol deficit. Cholesterol is a key component of mTORC1 activation²⁹, an event that requires mTORC1 localization to the surface of the lysosome³². In cells expressing Foxo1^{AAA}, we observed that lysosomal content decreased, a result consistent with diminished cholesterol levels^{29,30}. Thus, although decreased mTORC1 activity might contribute to anabolic defects, this process is likely to be a complex regulatory loop, not a simple ‘linear’ pathway. We also found that the immunological synapse formation of previously activated cells is impaired as a direct consequence of a cholesterol deficit. This finding suggests that metabolic responses of cells to an initial activation event modulate later proximal signaling events.

Despite the diminished mTORC1 activity, we observed hyperactivation of Akt. This result is especially notable, given the decreased expression of IL-2R β , because this subunit directly leads to PI3K³⁶. In agreement with this finding, under physiological stress, such as growth-factor limitations or reactive oxygen generation, Foxo1 can maintain high Akt and limit mTORC1 activity in mouse embryonic fibroblasts³⁷. However, although these effects have been shown to decrease anabolic metabolism, we found that catabolic energy-consuming pathways are also limited.

Perhaps most importantly, we found that activation of Akt takes place via a noncanonical pathway, because it occurs independently of mTORC2 activity and is not blocked by deletion of Rictor. This finding was striking, because mTORC2 is essential for activation of Akt in T cells³⁸. Several lines of evidence may account for this observation: altered signaling dynamics resulting from defective immunological synapse formation and CD3 expression; failure to recruit phosphatases to signaling platforms as a result of diminished PD-1 expression; decreased PTEN expression; and potentially loss of negative feedback from mTOR–S6K, a pathway that is well described in cancer cells³⁹. Further studies will be needed to determine why interference with Foxo1 inactivation abolishes the requirement of mTORC2 activity for Akt phosphorylation on Ser473.

Our data on CD4^{Cre} mice suggest that maintaining one copy of Foxo1^{AAA} severely disrupts T_{reg} cell ontogeny. This finding contrasts with those from a study in Foxp3^{Cre} mice, which has reported that maintaining one copy of Foxo1^{AAA} after T_{reg} cell differentiation inhibits effector T_{reg} function but does not interfere with naive T_{reg} cell homeostasis⁴⁰. Thus, although our data suggest a model of CD4 conventional T cell persistence in vivo that depends on oscillatory Foxo1 activity (to both allow growth-factor signals and support quiescence), after cell lineage commitment has been made, T_{reg} cells appear to tolerate prolonged continuance of Foxo1 activity. These differences in how Foxo1 activity modulates conventional CD4⁺ T cells and T_{reg} cells may be exploitable in the context of T cell–based gene therapies or adoptive cellular therapy.

Collectively, our data show that maintained Foxo1 transcriptional activity alters T cell responsiveness and competitive fitness. Although in a noncompetitive environment, cell proliferation is enhanced, this effect occurs in conjunction with decreases in cell biomass and cholesterol content. In vivo, this response results in a failure to maintain homeostasis and in CD4 T cells marked by defective ribosome biogenesis and cholesterol biosynthesis.

Together, these findings link the role of Foxos in controlling homing and migration with the coordination of growth and proliferation, and reveal how proper regulation of Foxos is critical to both maintaining tolerance and orchestrating immune responses.

Methods

Methods, including statements of data availability and any associated accession codes and references, are available at <https://doi.org/10.1038/s41590-018-0157-4>.

Methods

Mice.

Rosa26-flox-STOP-FOXO1^{AAA} (Foxo1^{AAA}) mice were generated and provided by M. Li⁸. CD4^{Cre}, CD45.1⁺ and *Rag1*^{-/-} mice were acquired from the Jackson laboratory. CD4^{Cre-ERT2} mice were generated and provided by F. Gounari⁴¹. *Rictor^{fl/fl}* mice have been described previously⁴². The experiments were not randomized; age-matched and, whenever possible, sex-matched littermate controls were used for all experiments. Unless otherwise noted, CD4^{Cre} Foxo1^{AAA/+} mice were used at 4–8 weeks of age. Other mice were used at 4–12 weeks of age unless otherwise noted. No statistical methods were used to predetermine sample size, which was determined on the basis of animal availability and experience with analysis of the immune system and the development of early-onset lethal autoimmunity. Experimental analyses were not blinded. For Cre induction with CD4^{Cre-ERT2} mice, 1 mg tamoxifen (Sigma-Aldrich) in corn oil was injected i.p. for five consecutive days and then either maintained for biweekly analysis of peripheral blood or analyzed 3 d after the last injection. All animals were cared for according to the guidelines of Massachusetts General Hospital and St. Jude's Children's Research Hospital, and the Institutional Animal Care and Use Committee approved all experimental protocols.

Bone marrow chimeras.

6- to 8-week-old recipient *Rag1*^{-/-} mice were sublethally irradiated (5 Gy) 16 h before retro-orbital transfer of 2×10^6 bone marrow cells from 4-week-old donors. Before transfer, bone marrow was depleted of CD3⁺ cells with a CD3e MicroBead Kit (Miltenyi) according to the manufacturer's instructions. For mixed bone marrow chimeras, an equal proportion (1×10^6 bone marrow cells each) of CD45.1⁺ wild-type bone marrow and CD45.2⁺ CD4^{Cre} Foxo1^{AAA/+} bone marrow was transferred.

Transcriptome analysis and bioinformatics-library preparation and sequencing.

cDNA was synthesized with Clontech SmartSeq v4 reagents from 250 pg of RNA. Full-length cDNA was fragmented to a mean size of 150 bp with a Covaris M220 ultrasonicator, and Illumina libraries were prepared from 2 ng of sheared cDNA with Rubicon Genomics ThruPLEX DNA-seq reagents according to the manufacturer's protocol. The finished dsDNA libraries were quantified with a Qubit fluorometer, Agilent TapeStation 2200 and RT-qPCR with a Kapa Biosystems Library Quantification Kit. Uniquely indexed libraries were pooled in equimolar ratios and sequenced on a single Illumina NextSeq500 run with single-end 75-bp reads by the Dana-Farber Cancer Institute Molecular Biology Core Facilities.

RNA-seq analysis.

Sequenced reads were aligned to the mm9 reference genome assembly, and gene counts were quantified with STAR (v2.5.1b). To identify genes differentially expressed between phenotypic groups, differential expression analysis was performed with the negative binomial generalized linear models implemented in the DESeq2 R package (Bioconductor). Gene-set enrichment analyses were performed with GSEAPreranked, in which genes were ranked according to their sign-corrected \log_{10} -adjusted P value and compared with the following MSigDB signature collections: curated hallmark gene sets, gene ontology biological processes and the c2 reactome^{43,44}. Functional analysis was performed with Database for Annotation, Visualization and Integrated Discovery (DAVID) bioinformatics resources⁴⁵. Gene expression array data from wild-type and Scurfy CD4 T cells were analyzed with GEO2R from GEO GSE11775 to select genes with twofold expression change ($P < 0.05$) for gene ontology with DAVID.

CD4 enrichment, cell sorting and in vitro T cell stimulations.

CD4 T cells were obtained from spleen and peripheral lymph nodes through negative selection with an EasySep mouse CD4 T cell Isolation Kit (StemCell Technologies) according to the manufacturer's instructions. Isolated CD4 T cells were stained with Live/Dead Fixable Dead Cell stain (Invitrogen) and the following fluorophoreconjugated antibodies from BioLegend: anti-CD4 (GK1.5), anti-CD25 (PC61), anti-CD44 (IM7) and anti-CD62L (MEL-14). GFP⁺ and GFP⁻ naïve CD4⁺ CD44^{lo}CD62L^{hi}CD25⁻ populations were sorted, cultured at 37°C and 5% CO₂ in complete RPMI 1640 medium and activated in vitro with plate-bound anti-CD3 (0.5 µg/ml; 145–2C11, BioLegend) and soluble anti-CD28 (0.2 µg/ml; 3751, BioLegend). To plate-bind anti-CD3, culture dishes were first coated with goat anti-hamster (7 µg/ml, Vector Labs) in carbonate buffer (50 mM sodium carbonate and 50 mM sodium bicarbonate, pH 9.5). To measure cell proliferation and survival, sorted cells were labeled with CellTrace Violet (Invitrogen) before being cultured with plate-bound anti-CD3 and soluble anti-CD28; before flow cytometry, cells were stained with either 7AAD (eBioscience) or Live/Dead Fixable Dead Cell stain. For IL-2 withdrawal assays, anti-IL-2 blocking antibody (JES6–1A12, BioLegend) was used. For inhibition of dynamin- and clathrin-mediated endocytosis, Dynasore (Sigma-Aldrich) was used.

Flow cytometry.

In vitro-cultured cells or cells isolated from lymphoid organs from mice were collected, resuspended in staining buffer (PBS containing 2% FBS) and stained. The following antibodies from BioLegend were used: anti-CD4 (GK1.5), anti-CD8 (53–6.7), anti-CD44 (IM7), anti-PD-1 (29 F.1A12), anti-Ki-67 (16A8), anti-Bcl-2 (100), anti-IL7R α (A7R34), anti-CD3 (17A2), anti-CD19 (6D5), anti-IgM (RMM-1), anti-IgD (1126 c.2a), anti-CD25 (PC61), anti-CD122 (5H4), anti-CD132 (TUGm2), anti-CD45.1 (A20), anti-CD45.2 (104), anti-BrdU (Bu20a), anti-IFN- γ (XMG1.2), anti-granzyme B (GB11), anti-IL-4 (11B11), anti-MHC II I-Ab (AF6–120.1), anti-CD40 (3/23), anti-ICOS (7E.17G9), anti-CTLA-4 (UC10–4B9) and fluorophore-conjugated polyclonal anti-rabbit. Fluorophore-conjugated streptavidin was also from BioLegend. The following antibodies from eBioscience were used: anti-B7–1 (16–10A1), anti-Foxp3 (FJK-16s), anti-GL-7 (GL-7), anti-Fas (15A7) and

biotin-conjugated anti-CXCR5 (SPRCL5). Anti-IL2 (JES6-5H4) was from BD Biosciences. For intracellular staining, a Foxp3 fix/perm kit (eBioscience) was used after surface staining. Intracellular staining of Myc was performed with anti-Myc (D84C12) from Cell Signaling. For staining of phosphorylated proteins, cells were fixed in 2% PFA and then permeabilized in 100% ice-cold MeOH. The following primary and secondary antibodies were stained in PBS containing 2% FBS: unconjugated anti-p-Akt Ser473 (D9E, Cell Signaling), fluorophoreconjugated polyclonal anti-rabbit (BioLegend) and fluorophore-conjugated anti-p-STAT5 Tyr694 (SRBCZX, eBioscience). All flow cytometry was analyzed with a Navios (Beckman Coulter) flow cytometer with standard filter sets and FlowJo software (TreeStar), except when a 561-nM laser was needed for RFP detection, for which an LSR II (Becton Dickson) was used.

In vivo BrdU labeling.

8- to 12-week-old mice that had received five daily, consecutive injections of tamoxifen 2 weeks earlier were injected with 1 mg BrdU in PBS every 12 h for three consecutive days. Cells that incorporated BrdU were detected with a BrdU Flow Kit (BD Biosciences) according to the manufacturer's instructions.

Retroviral transduction of T cell cultures.

The retroviral constructs MSCV-IRES-RFP (MIR and MIR-Myc) and MSCV-IRES-Thy1.1 (MIT and MIT-caSTAT5b) were packaged in HEK 293 T cells maintained in DMEM supplemented with 10% FBS with the helper plasmids pHIT-60 and pHIT-123. To produce virus, HEK 293 T cells were transfected with constructs and helper plasmids with Lipofectamine 3000 reagent (Promega) according to the manufacturer's instructions. 12 h after transfection, the supernatant was removed, discarded and replaced with fresh DMEM; 12 h later, the medium was replaced with RPMI complete medium and collected and replaced every 12 h for the next 48 h. For retroviral transductions, sorted cells were activated for 24 h with plate-bound anti-CD3 and soluble anti-CD28. Cells were then treated with viral supernatant containing 4 µg/ml polybrene and centrifuged at 500 *g* for 1 h. 24 h after transduction, medium containing viral supernatant was removed and replaced with fresh RPMI complete medium, and 48 h after transduction, cells were analyzed by flow cytometry.

Immunofluorescence imaging of Filipin III staining.

Day 2 T cell cultures were adhered to Nunc glass-bottom cell culture dishes with Cell-Tak (BD Bioscience), fixed with 2% paraformaldehyde and stained with Filipin III (45 min at room temperature, 50 µg/ml final concentration). After being washed with PBS, stained cells were imaged with a Zeiss LSM710 confocal microscope and analyzed with ZEN software (Zeiss).

Immunofluorescence imaging of mTOR and lysosomes.

Day 2 T cell cultures were adhered to Nunc glass-bottom cell culture dishes with Cell-Tak (BD Bioscience), then further incubated for an additional 2 h at 37°C and 5% CO₂ in unsupplemented RPMI medium (Gibco) or RPMI medium supplemented with 11.1 mM

glucose (Sigma), 10% FBS and RPMI 1640 amino acids solution (Sigma). Cells were fixed with 2% paraformaldehyde, then permeabilized and blocked with 2% normal goat serum (Jackson ImmunoResearch) and 0.05% saponin (Sigma) in PBS at room temperature for 2 h. Primary-antibody staining for Lamp-1 (Developmental Studies Hybridoma Bank; 1D4B) and mTOR (Cell Signaling Technology; 7C10) was performed overnight at 4°C and was followed by washing in perm/blocking buffer and secondary-antibody staining (Invitrogen; goat anti-rabbit IgG (H + L) Alexa Fluor 647 and goat anti-rat IgG (H + L) Alexa Fluor 594) for 1 h at room temperature in perm/blocking buffer. After being washed with PBS, stained cells were mounted in Fluoro-Gel II mounting medium containing DAPI (Electron Microcopy Sciences) and were imaged with a Zeiss LSM710 confocal microscope and analyzed with ZEN software (Zeiss).

Histology and immunohistochemistry.

For analysis of pathology and immune cell infiltration into nonlymphoid organs, tissue was fixed with 10% formalin, paraffin embedded, sectioned and stained with hematoxylin and eosin. For staining of IgG deposition in kidneys, 6- μ M-thick frozen sections of OCT-embedded kidneys were fixed with 3.2% formaldehyde (Polysciences), permeabilized in 90% methanol and incubated with blocking buffer (2% goat serum, 1% BSA, 0.1% cold fish skin gelatin, 0.1% saponin and 0.05% Tween-20 in 0.01 M PBS). Tissues were stained with Alexa 488-conjugated goat anti-mouse IgG (H + L) (Thermo Fisher). Fluorescence images were acquired with a Leica TCS SP5 II confocal microscope and Leica Acquisition Software. For autoantibody (ANA) staining, fixed HEp-2 ANA slides (MBL) were stained with PBS-diluted serum (1:50). Slides were washed and stained with either Alexa 488-conjugated goat anti-mouse IgG (H + L) or Alexa 568-conjugated goat anti-mouse IgM (Thermo Fisher) as detection antibodies. Fluorescence images were acquired with a Leica TCS SP5 II confocal microscope and Leica Acquisition Software.

Antibody quantification and ELISA.

Immunoplate MaxiSorp plates (Thermo Fisher) were coated with 10 μ g/ml goat anti-mouse IgG (heavy and light chain specific; Southern Biotech) in PBS at 4°C overnight. Plates were blocked with 1% BSA in PBS, washed and then incubated with diluted sera in PBS or standards. Plates were then incubated with 1:1,000 diluted alkaline phosphatase-conjugated IgM, IgG, or IgG1 (Southern Biotech). Secondary antibodies were detected by disodium *p*-nitrophenyl phosphate substrate (Sigma-Aldrich), and absorbance (OD) was read at 405 nm.

Blood and serum glucose analysis.

Blood glucose was measured via saphenous vein blood collection, and levels were determined with an Ascensia Contour blood glucose meter and blood glucose monitoring strips (Bayer Healthcare). Red blood cell percentages were determined after heart-puncture blood collection. Blood was collected into microhematocrit tubes and spun for 120 s with a CritSpin StatSpin centrifuge (Iris Sample Processing). Separated serum and red blood cell percentages were determined with a Micro Hematocrit Capillary Tube Reader (StatSpin, Iris Sample Processing).

RNA isolation and qPCR.

RNA was isolated with an RNeasy Plus Micro Kit (Qiagen). For qPCR, RNA was converted to cDNA with iScript Reverse Transcription Supermix (Bio-Rad) and measured with RT² SYBR Green ROX qPCR Mastermix (Qiagen). Samples were run in duplicate or triplicate on an MX3005P qPCR system (Stratagene), analyzed with MXPro qPCR software (Stratagene) and normalized to β -actin. Primer sequences for the following genes (NCBI gene symbol, PrimerBank ID) were obtained from PrimerBank (<http://pga.mgh.harvard.edu/primerbank/>): *Idi1*, 21703726a1; *Fdps*, 19882207a1; *Ldlr*, 6754526a1; *Sqle*, 6678127a1; *Cyp51*, 9910172a1; *Dhcr24*, 16716609a1; *Hmgcr*, 26347907a1; *Acaca*, 14211280a1; *Fasn*, 30911099a1; *Mvk*, 12963731a1; *Myc*, 27545183a1; *Il2*, 7110653a1; and *Actb*, 6671509a1.

Immunoblotting.

Cells were lysed in RIPA buffer (150 mM NaCl, 1% NP-40, 0.5% sodium deoxycholate, 0.1% sodium dodecyl sulfate, 50 mM Tris, 1 mM EDTA and 1 mM EGTA), and immunoblotting was performed with standard procedures. Antibodies specific to the following proteins were obtained from Cell Signaling Technologies: Myc (D84C12), p-Akt Thr308 (C31E5E), p-Akt Ser473 (D9E), Akt (9272), p-S6 Ser235/236 (D57.2.2E), S6 (5G10), p-4E-BP1 Thr37/46 (236B4), p-mTOR Ser2448 (D9C2), p-PKC α/β Thr638/641 (9375), p-Ndr1 Thr346 (D98G11), p-Jak1 Tyr1034/1035 (D7N4Z), p-Stat5 Tyr694 (D47E7), p-Pdk1 Ser241 (C49H2), Rictor (53 A2), LC-3A/B (D3U4C) and β -actin (D6A8). An Hif-1 α -specific polyclonal antibody (10006421) was from Cayman Chemical, anti-Lamp-1 (1D4B) was from the Developmental Studies Hybridoma Bank, and anti-PTEN (6H2.1) was from Cascade Bioscience. Horseradish peroxidase-conjugated goat anti-rabbit IgG (Bio-Rad) was used as a secondary antibody. 5% milk in PBS with 0.1% Tween 2-0 was used as blocking buffer.

Metabolic assays.

OCR and ECAR were measured with an XF96 extracellular flux analyzer (Seahorse Bioscience) according to the manufacturer's protocols. FACS-sorted T cells from day 3 cultures were attached to culture plates with Cell-Tak (BD Bioscience) and were maintained in nonbuffered assay medium in a non-CO₂ incubator for 1 h before the assay. A Glycolysis Stress Test Kit (Seahorse Bioscience) was used to monitor ECAR in assay medium supplemented with 10 mM l-glutamine (HyClone). Three baseline recordings were made, and this was followed by sequential injection of glucose (10 mM), the mitochondrial/ATP synthase inhibitor oligomycin (3 μ M) and the glycolysis inhibitor 2-deoxy-d-glucose (100 mM). Glycolytic capacity was defined as the difference between the ECAR after the injection of oligomycin and the basal ECAR. A Mito Stress Test Kit (Seahorse Bioscience) was used to assay the mitochondrial respiration rate with assay medium supplemented with 10 mM l-glutamine and 10 mM d-glucose (Sigma-Aldrich). Three baseline recordings were made, and this was followed by sequential injection of the ATP synthase inhibitor oligomycin (3 μ M), the mitochondrial uncoupler carbonyl cyanide-4-(trifluoromethoxy)phenyl-hydrazone (FCCP; 1 μ M) and the respiratory chain inhibitors antimycin A (1.5 μ M) and rotenone (3 μ M). Mitochondrial respiratory capacity was defined as the difference between the OCR after the injection of FCCP and the basal OCR. Glucose

and glutamine consumption, and lactate and glutamate production, were measured in cell supernatants obtained at days 2 and 3 of cultures with a BioProfile Flex Analyzer (Nova Biomedical).

Supported lipid bilayer and total internal reflection fluorescence microscope imaging.

SLBs were formed as previously described²³. In brief, glass coverslips were cleaned with piranha solution (30% H₂O₂ and 70% H₂SO₄), rinsed extensively, dried, negatively charged through plasma cleaning, and assembled with a six-channel sticky-Slide VI 0.4 (Ibidi). SLBs were formed by filling each channel with a suspension of small unilamellar vesicles composed of 1,2-dioleoyl-*sn*-glycero-3-[*N*-(5-amino-1-carboxypentyl) succinyl] (12.5% mol) and 1,2-dioleoyl-*sn*-glycero-3-phosphoethanolamine-*N*-cap biotinyl (0.05% mol) in 1,2-dioleoyl-*sn*-glycero-3-phosphocholine at a total lipid concentration of 0.4 mM (Avanti Polar Lipids). SLBs were blocked with 5% casein (Sigma), 10% human serum albumin (Calbiochem), 100 μM NiSO₄ and HEPES-buffered saline solution, then incubated with 5 μg/ml unlabeled streptavidin for 20 min and then with concentrations of Alexa Fluor 568–conjugated monobiotinylated anti-mouse TCR V α 1.1 (clone 2C11) (30 molecules/μM²), histidine-tagged Alexa Fluor 405–conjugated mouse ICAM-1 (200 molecules/μM²) and Alexa Fluor 647–conjugated human CD80 (100 molecules/μM²) titrated to obtain indicated densities after a 20-min incubation. Mouse CD4 T cells were sorted after 3 d of activation by plate bound anti-CD3/CD28 in GFP⁺ (ca-Foxo1) and GFP (wild type) populations; rested for at least 6 h at 37°C in 25 U/ml rhIL-2 (Immunotools); and incubated for 10 min. at 37°C on prewarmed SLBs. T cells were fixed with 4% paraformaldehyde in 60 mM PIPES, 25 mM HEPES, 10 mM EGTA, 4 mM MgCl₂ (PHEM buffer), pH 7, extensively washed and subsequently imaged on an Olympus IX83 inverted microscope equipped with Olympus UApON 150 \times , 1.45-NA objective, 405-, 568-, 647-nm argon laser, and an Evolve delta EMCDD camera. Successful immunological synapse formation was blindly scored as the percentage of SLB-bound T cells with a cSMAC defined as location with dense 2C11 and exclusion of ICAM-1. IRM was used to determine the T cell–SLB interaction surface area. This area was used as a mask in Fiji⁴⁶ to determine the recruitment of TCR and LFA-1, as determined by the integrated densities of 2C11 and ICAM-1.

Cholesterol administration before imaging.

Mouse CD4 T cells were incubated with culture medium (RPMI 1640, 5% FBS, pen/strep and l-glutamine; all from Gibco) supplemented with 10 μg/ml M β CD-coated cholesterol at 37°C for 15 min. The cells were washed three times with 37°C PBS (Gibco), resuspended in culture medium and finally incubated on SLBs.

Filipin III staining for immunological synapse imaging.

Filipin III (Sigma) was dissolved in ethanol to a final concentration of 5 mg/ml. Cells were fixed with 4% paraformaldehyde in PHEM buffer, pH 7, extensively washed and stained with 50 μg/ml Filipin III for 30 min at 4°C. After three washes with 4°C PBS, cells were placed in glass-bottom eight-well μ -well slides (Ibidi) and imaged on an Olympus confocal microscope. The integrated density of Filipin was determined in Fiji.

Statistical analysis.

All statistical analyses were performed in Prism software (GraphPad). Data were analyzed with two-tailed, unpaired Student's *t* tests to determine whether two means were significantly different, and $P < 0.05$ was considered significant, unless otherwise indicated. The variance was similar between groups being statistically compared.

Reporting Summary.

Further information on experimental design is available in the Nature Research Reporting Summary linked to this article.

Data availability.

The data that support the findings of this study are available from the corresponding author upon reasonable request.

Supplementary Material

Refer to Web version on PubMed Central for supplementary material.

Acknowledgements

We thank M. Li (Memorial Sloan Kettering Cancer Center) for Foxo1^{AAA} mice; F. Gounari (University of Chicago) for CD4^{Cre-ERT2} mice; M. Farrar (University of Minnesota) for a constitutively active STAT5b retroviral construct; Z. Herbert and K. Bi for assistance with transcriptome analysis; the MGH-CNY FACS core facility for cell sorting; and members of the laboratory of L.A.T. for discussions. This work was supported by the US National Institutes of Health (P01HL018646 to L.A.T.; R21AI126143 to L.A.T. and R.H.N.; R01AI124693 to D.J.C.; R01HL011879 and P01AI056299 to B.R.B.; AI101407 and CA176624 to H.C.), the Wellcome Trust (PRF 100262 to M.L.D.) and the European Research Council (ERC-2014-AdG_670930 to M.L.D. and E.B.C.).

References

1. Manning BD & Toker A AKT/PKB signaling: navigating the network. *Cell* 169, 381–405 (2017). [PubMed: 28431241]
2. Liao W, Lin JX & Leonard WJ Interleukin-2 at the crossroads of effector responses, tolerance, and immunotherapy. *Immunity* 38, 13–25 (2013). [PubMed: 23352221]
3. Smith-Garvin JE, Koretzky GA & Jordan MS T cell activation. *Annu. Rev. Immunol* 27, 591–619 (2009). [PubMed: 19132916]
4. Kerdiles YM et al. Foxo1 links homing and survival of naive T cells by regulating L-selectin, CCR7 and interleukin 7 receptor. *Nat. Immunol* 10, 176–184 (2009). [PubMed: 19136962]
5. Ouyang W, Beckett O, Flavell RA & Li MO An essential role of the Forkhead-box transcription factor Foxo1 in control of T cell homeostasis and tolerance. *Immunity* 30, 358–371 (2009). [PubMed: 19285438]
6. Kerdiles YM et al. Foxo transcription factors control regulatory T cell development and function. *Immunity* 33, 890–904 (2010). [PubMed: 21167754]
7. Ouyang W et al. Foxo proteins cooperatively control the differentiation of Foxp3⁺ regulatory T cells. *Nat. Immunol* 11, 618–627 (2010). [PubMed: 20467422]
8. Ouyang W et al. Novel Foxo1-dependent transcriptional programs control T_{reg} cell function. *Nature* 491, 554–559 (2012). [PubMed: 23135404]
9. Zeng H et al. mTORC1 couples immune signals and metabolic programming to establish T_{reg}-cell function. *Nature* 499, 485–490 (2013). [PubMed: 23812589]

10. Yang K et al. T cell exit from quiescence and differentiation into Th2 cells depend on Raptor-mTORC1-mediated metabolic reprogramming. *Immunity* 39, 1043–1056 (2013). [PubMed: 24315998]
11. Kuczma M et al. Foxp3-deficient regulatory T cells do not revert into conventional effector CD4⁺ T cells but constitute a unique cell subset. *J. Immunol* 183, 3731–3741 (2009). [PubMed: 19710455]
12. Kousteni S FoxO1, the transcriptional chief of staff of energy metabolism. *Bone* 50, 437–443 (2012). [PubMed: 21816244]
13. Webb AE, Kundaje A & Brunet A Characterization of the direct targets of FOXO transcription factors throughout evolution. *Aging Cell* 15, 673–685 (2016). [PubMed: 27061590]
14. Wilhelm K et al. FOXO1 couples metabolic activity and growth state in the vascular endothelium. *Nature* 529, 216–220 (2016). [PubMed: 26735015]
15. Sinclair LV et al. Control of amino-acid transport by antigen receptors coordinates the metabolic reprogramming essential for T cell differentiation. *Nat. Immunol* 14, 500–508 (2013). [PubMed: 23525088]
16. Wang R et al. The transcription factor Myc controls metabolic reprogramming upon T lymphocyte activation. *Immunity* 35, 871–882 (2011). [PubMed: 22195744]
17. Lord JD, McIntosh BC, Greenberg PD & Nelson BH The IL-2 receptor promotes proliferation, bcl-2 and bcl-x induction, but not cell viability through the adapter molecule Shc. *J. Immunol* 161, 4627–4633 (1998). [PubMed: 9794391]
18. Preston GC et al. Single cell tuning of Myc expression by antigen receptor signal strength and interleukin-2 in T lymphocytes. *EMBO J.* 34, 2008–2024 (2015). [PubMed: 26136212]
19. Buck MD, O’Sullivan D & Pearce EL T cell metabolism drives immunity. *J. Exp. Med* 212, 1345–1360 (2015). [PubMed: 26261266]
20. MacIver NJ, Michalek RD & Rathmell JC Metabolic regulation of T lymphocytes. *Annu. Rev. Immunol* 31, 259–283 (2013). [PubMed: 23298210]
21. Dustin ML The immunological synapse. *Cancer Immunol. Res* 2, 1023–1033 (2014). [PubMed: 25367977]
22. Yang W et al. Potentiating the antitumour response of CD8⁺ T cells by modulating cholesterol metabolism. *Nature* 531, 651–655 (2016). [PubMed: 26982734]
23. Choudhuri K et al. Polarized release of T-cell-receptor-enriched microvesicles at the immunological synapse. *Nature* 507, 118–123 (2014). [PubMed: 24487619]
24. Brunet A et al. Protein kinase SGK mediates survival signals by phosphorylating the forkhead transcription factor FKHRL1 (FOXO3a). *Mol. Cell. Biol* 21, 952–965 (2001). [PubMed: 11154281]
25. Feng J, Park J, Cron P, Hess D & Hemmings BA Identification of a PKB/Akt hydrophobic motif Ser-473 kinase as DNA-dependent protein kinase. *J. Biol. Chem* 279, 41189–41196 (2004). [PubMed: 15262962]
26. Xu C et al. Regulation of T cell receptor activation by dynamic membrane binding of the CD3epsilon cytoplasmic tyrosine-based motif. *Cell* 135, 702–713 (2008). [PubMed: 19013279]
27. Hui E et al. T cell costimulatory receptor CD28 is a primary target for PD-1-mediated inhibition. *Science* 355, 1428–1433 (2017). [PubMed: 28280247]
28. Sancak Y et al. Ragulator-Rag complex targets mTORC1 to the lysosomal surface and is necessary for its activation by amino acids. *Cell* 141, 290–303 (2010). [PubMed: 20381137]
29. Castellano BM et al. Lysosomal cholesterol activates mTORC1 via an SLC38A9-Niemann-Pick C1 signaling complex. *Science* 355, 1306–1311 (2017). [PubMed: 28336668]
30. Marschner K, Kollmann K, Schweizer M, Bräulke T & Pohl S A key enzyme in the biogenesis of lysosomes is a protease that regulates cholesterol metabolism. *Science* 333, 87–90 (2011). [PubMed: 21719679]
31. Hecht VC et al. Biophysical changes reduce energetic demand in growth factor-deprived lymphocytes. *J. Cell Biol* 212, 439–447 (2016). [PubMed: 26880201]
32. Sancak Y et al. The Rag GTPases bind raptor and mediate amino acid signaling to mTORC1. *Science* 320, 1496–1501 (2008). [PubMed: 18497260]

33. Efeyan A et al. Regulation of mTORC1 by the Rag GTPases is necessary for neonatal autophagy and survival. *Nature* 493, 679–683 (2013). [PubMed: 23263183]
34. Verbist KC et al. Metabolic maintenance of cell asymmetry following division in activated T lymphocytes. *Nature* 532, 389–393 (2016). [PubMed: 27064903]
35. Laplante M & Sabatini DM mTOR signaling in growth control and disease. *Cell* 149, 274–293 (2012). [PubMed: 22500797]
36. Brennan P et al. Phosphatidylinositol 3-kinase couples the interleukin-2 receptor to the cell cycle regulator E2F. *Immunity* 7, 679–689 (1997). [PubMed: 9390691]
37. Chen CC et al. FoxOs inhibit mTORC1 and activate Akt by inducing the expression of Sestrin3 and Rictor. *Dev. Cell* 18, 592–604 (2010). [PubMed: 20412774]
38. Delgoffe GM et al. The kinase mTOR regulates the differentiation of helper T cells through the selective activation of signaling by mTORC1 and mTORC2. *Nat. Immunol* 12, 295–303 (2011). [PubMed: 21358638]
39. Zoncu R, Efeyan A & Sabatini DM mTOR: from growth signal integration to cancer, diabetes and ageing. *Nat. Rev. Mol. Cell Biol* 12, 21–35 (2011). [PubMed: 21157483]
40. Luo CT, Liao W, Dadi S, Toure A & Li MO Graded Foxo1 activity in T_{reg} cells differentiates tumour immunity from spontaneous autoimmunity. *Nature* 529, 532–536 (2016). [PubMed: 26789248]
41. Aghajani K, Keerthivasan S, Yu Y & Gounari F Generation of CD4CreER(T2) transgenic mice to study development of peripheral CD4-T-cells. *Genesis* 50, 908–913 (2012). [PubMed: 22887772]
42. Yang K, Neale G, Green DR, He W & Chi H The tumor suppressor Tsc1 enforces quiescence of naive T cells to promote immune homeostasis and function. *Nat. Immunol* 12, 888–897 (2011). [PubMed: 21765414]
43. Liberzon A et al. Molecular signatures database (MSigDB) 3.0. *Bioinformatics* 27, 1739–1740 (2011). [PubMed: 21546393]
44. Subramanian A et al. Gene set enrichment analysis: a knowledge-based approach for interpreting genome-wide expression profiles. *Proc. Natl. Acad. Sci. USA* 102, 15545–15550 (2005). [PubMed: 16199517]
45. Huang W, Sherman BT & Lempicki RA Systematic and integrative analysis of large gene lists using DAVID bioinformatics resources. *Nat. Protoc* 4, 44–57 (2009). [PubMed: 19131956]
46. Schindelin J et al. Fiji: an open-source platform for biological-image analysis. *Nat. Methods* 9, 676–682 (2012). [PubMed: 22743772]

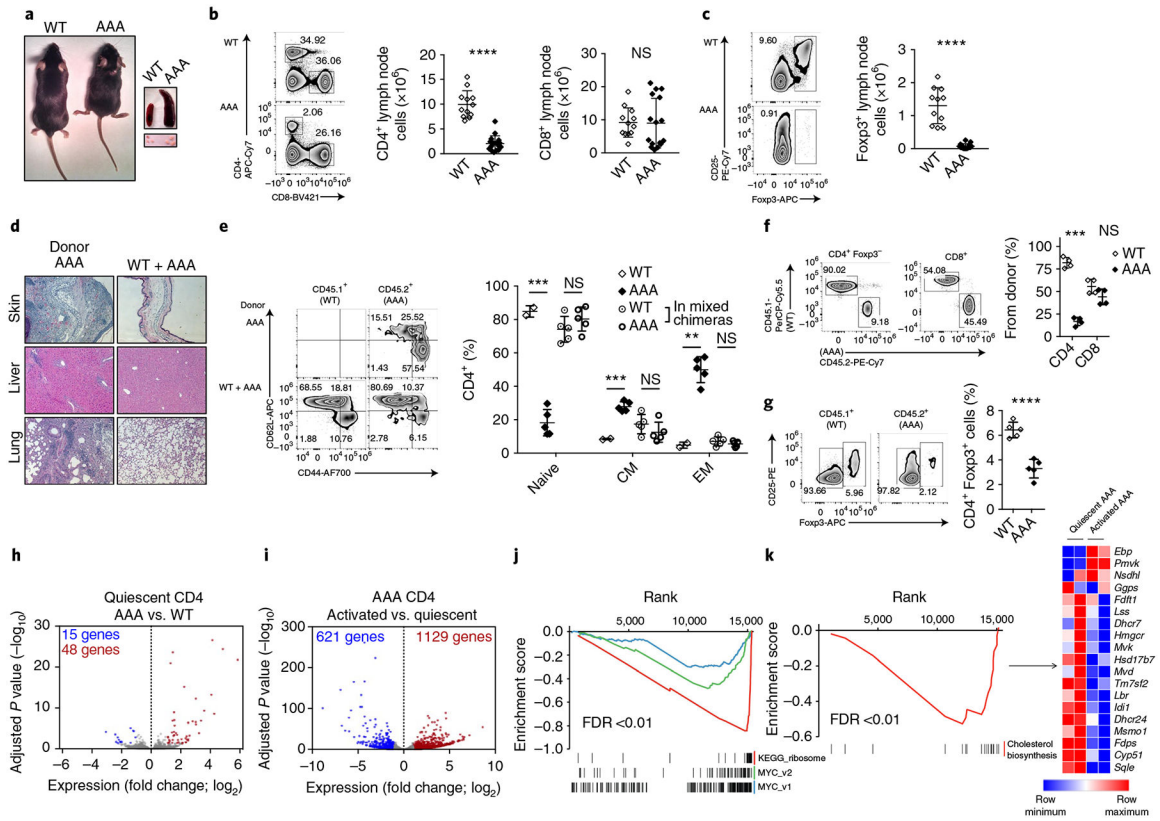


Fig. 1 | Autoimmunity in mice with T cell-specific dysregulation of Foxo1 activity.

a, Representative images of 8-week-old CD4^{Cre} Foxo1^{AAA/+} (AAA) and CD4^{Cre} Foxo1^{+/+} (WT) littermates, seen consistently in a large cohort (> 20 mice). Right, spleen and lymph nodes. Quantification in Supplementary Fig. 1a,b. **b**, Flow cytometric analysis of lymph node cells from 8-week-old WT and AAA littermates (left) and quantification of numbers of CD4⁺ and CD8⁺ T cells from lymph nodes of 4- to 8-week-old mice (*n* = 12 mice). **c**, Flow cytometric analysis of CD4⁺ T cells from lymph nodes from 6-week-old WT and AAA littermates (left) and quantification of frequencies and numbers of Foxp3⁺CD4⁺ T_{reg} cells from 4- to 8-week-old mice (*n* = 11 mice). **d**, Hematoxylin and eosin staining of liver, lung and ear skin (original magnification, 10×) in bone marrow chimeras 10 weeks post-transfer. *Rag1*^{-/-} recipients were sublethally irradiated before receiving bone marrow cells from WT donors (CD45.1⁺) and/or CD4^{Cre} Foxo1^{AAA/+} (AAA) donors (CD45.2⁺). For mixed chimeras (WT + AAA), equal proportions of bone marrow cells were cotransferred. Results are representative of three independent experiments with similar results. **e**, Flow cytometric analysis of CD4⁺ T cells from the blood of bone marrow chimeras 10 weeks post-transfer (left) and quantification of the proportions of CD4⁺ naïve (CD44^{lo}CD62L^{hi}), central memory (CM; CD44^{hi}CD62L^{hi}) and effector memory (EM; CD44^{hi}CD62L^{lo}) cells from the blood of bone marrow chimeras 10 weeks post-transfer (right; WT, *n* = 2 mice; AAA, *n* = 5; WT + AAA chimeras, *n* = 5). **f**, Flow cytometric analysis of CD4⁺ and CD8⁺ T cells from the blood of bone marrow chimeras 10 weeks post-transfer (left) and quantification of the proportions of CD4⁺ and CD8⁺ T cells from the spleen 12 to 15 weeks post-transfer (right; *n* = 4 mice). **g**, Flow cytometric analysis of CD4⁺ T cells from the blood of bone marrow

chimeras 10 weeks post-transfer (left) and quantification of the proportion of Foxp3⁺CD4⁺ T_{reg} cells from the blood 10 weeks post-transfer (right; $n = 5$ mice). For **b**, **c** and **e–h**, quantification involved a two-tailed Student's t test with no adjustments made for multiple comparisons; center value, mean; error bars, s.d.; ** $P < 0.005$; *** $P < 0.0005$; **** $P < 0.0001$; NS, not significant. **h,i**, Volcano plots showing differential expression in CD4⁺ AAA (GFP⁺CD45.2⁺) versus WT (GFP⁻CD45.1⁺) CD62L^{hi}CD44^{lo} (quiescent) populations from spleens of mixed bone marrow chimeras (**h**), and CD4⁺ AAA (GFP⁺CD45.2⁺) CD62L^{lo}CD44^{hi} (activated) cells from single chimeras that received only AAA bone marrow versus CD4⁺ AAA (GFP⁺CD45.2⁺) CD62L^{hi}CD44^{lo} (quiescent) cells from mixed chimeras (**i**). Genes represented in blue and red have a log₂ fold change of < -1 , and > 1 , respectively, and an adjusted P value < 0.05 . One data point in **h** (*Ctse*; log₂ fold change, -5.19 ; $-\log_{10}$ adjusted P value, 121.5) is outside the axis limits to depict the dataset more clearly. **j,k**, Gene-set enrichment analysis showing underrepresentation of genes involved in Myc signaling and ribosome biogenesis (**j**) and cholesterol biosynthesis (**k**), in activated versus quiescent AAA CD4 T cells, as in **i** above. The heat map on the right (in **k**) displays the row minimum and maximum values of expression for the entire reactome cholesterol-biosynthesis annotated gene set. The log₁₀ Benjamini–Hochberg-adjusted P values were used, corrected for the direction of fold change, to rank genes. For any adjusted P -value cutoff, Benjamini–Hochberg correction was used. FDR, false discovery rate.

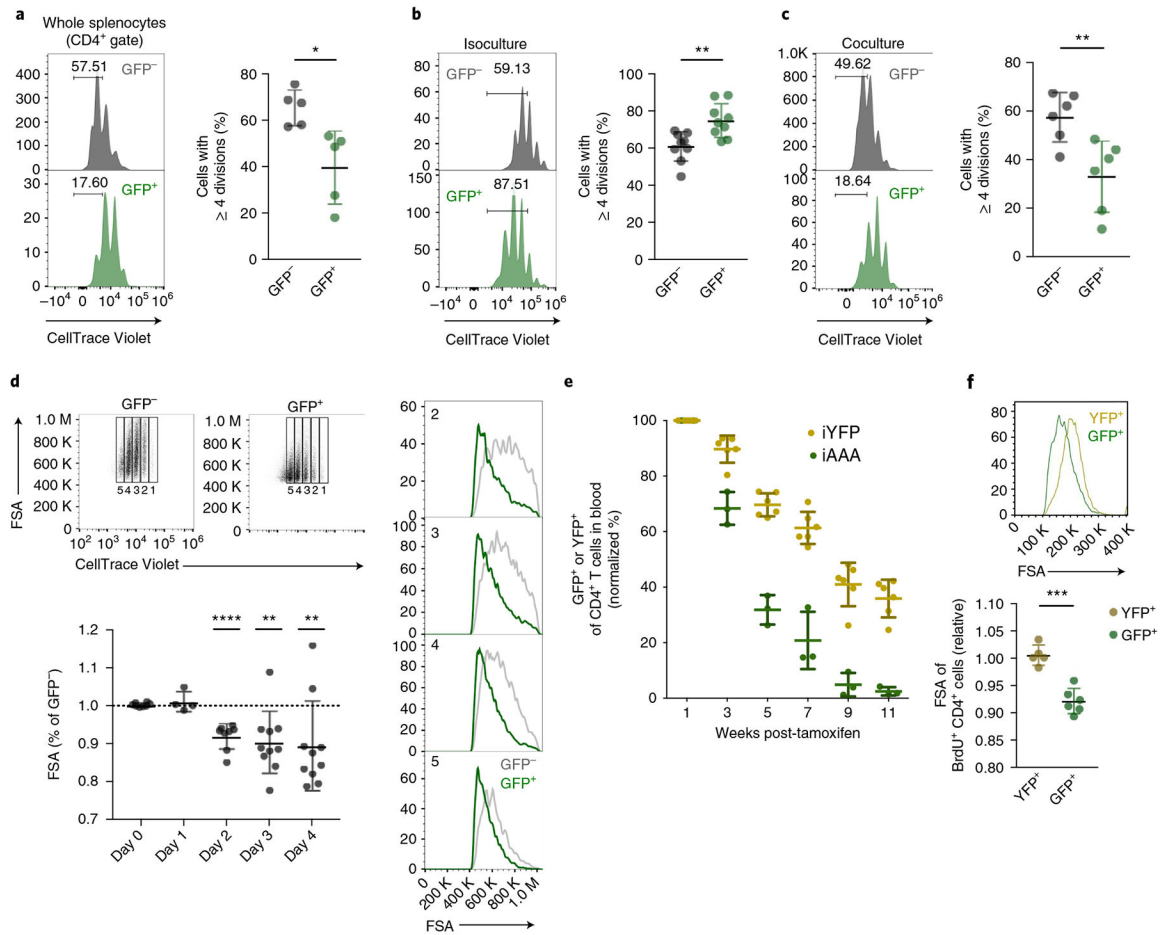


Fig. 2 | Foxo1 dysregulation uncouples cell growth and proliferation.

a-c, Flow cytometric analysis of CellTrace Violet dilutions of GFP⁻ (WT) and GFP⁺ (AAA) CD4⁺ T cells from CD4^{Cre-ERT2} Foxo1^{AAA/+} (iAAA) mice after 3 d in culture with plate-bound anti-CD3 and soluble anti-CD28. Tamoxifen was administered to CD4^{Cre-ERT2} Foxo1^{AAA/+} mice for four to five consecutive days starting from day 0, and spleens and lymph nodes were harvested at days 7 or 8. **a**, CD4⁺ gate of whole splenocytes ($n = 5$ mice). No sorting was performed on cells harvested from tamoxifen-treated mice before plating. **b,c**, Harvested lymphocytes were sorted to obtain both GFP⁻ and GFP⁺ naive cells (CD4⁺CD25⁻CD44^{lo}CD62L^{hi}). For isolated cultures (isocultures; **b**, $n = 8$), each population was plated in separate wells for the duration of the experiment in vitro, and cocultures (**c**, $n = 6$) combined GFP⁻ and GFP⁺ populations at a 5:1 ratio. **d**, Flow cytometric analysis of 4-day cultures, activated as in **b**, with gating on all generations to compare differences in cell size, as measured by forward-scatter area (FSA), and quantification of FSA, depicting GFP⁺ mean FSA as a percentage of mean FSA in control GFP⁻ cells for each given day (day 0, $n = 6$; day 1, $n = 4$; day 2, $n = 6$; days 3 and 4, $n = 10$). **e**, Persistence of AAA⁺ cells in vivo after tamoxifen treatment. Tamoxifen was administered to both CD4^{Cre-ERT2} Foxo1^{AAA/+} (iAAA; $n = 3$ mice) and CD4^{Cre-ERT2} Rosa26^{YFP/+} (iYFP; $n = 6$ mice) control mice for five consecutive days, and the percentage of GFP⁺ cells (from iAAA mice) and YFP⁺ cells (from iYFP mice) was followed in the blood for 11 weeks. All mice were 20–22 weeks old before

tamoxifen administration to minimize dilution of induced populations via strong thymic output. **f**, After administration of tamoxifen to mice (8–12 weeks old) as in **e**, bromodeoxyuridine (BrdU) was injected every 12 h for three consecutive days, beginning 2 weeks post-tamoxifen. Spleens were harvested, and CD4⁺ BrdU⁺ cells (shown in histograms) were analyzed for cell size according to FSA ($n = 6$). For all graphs, quantification involved a two-tailed Student's *t* test with no adjustments made for multiple comparisons; center value, mean, error bars, s.d. * $P < 0.05$; ** $P < 0.005$; *** $P < 0.0005$; **** $P < 0.0001$.

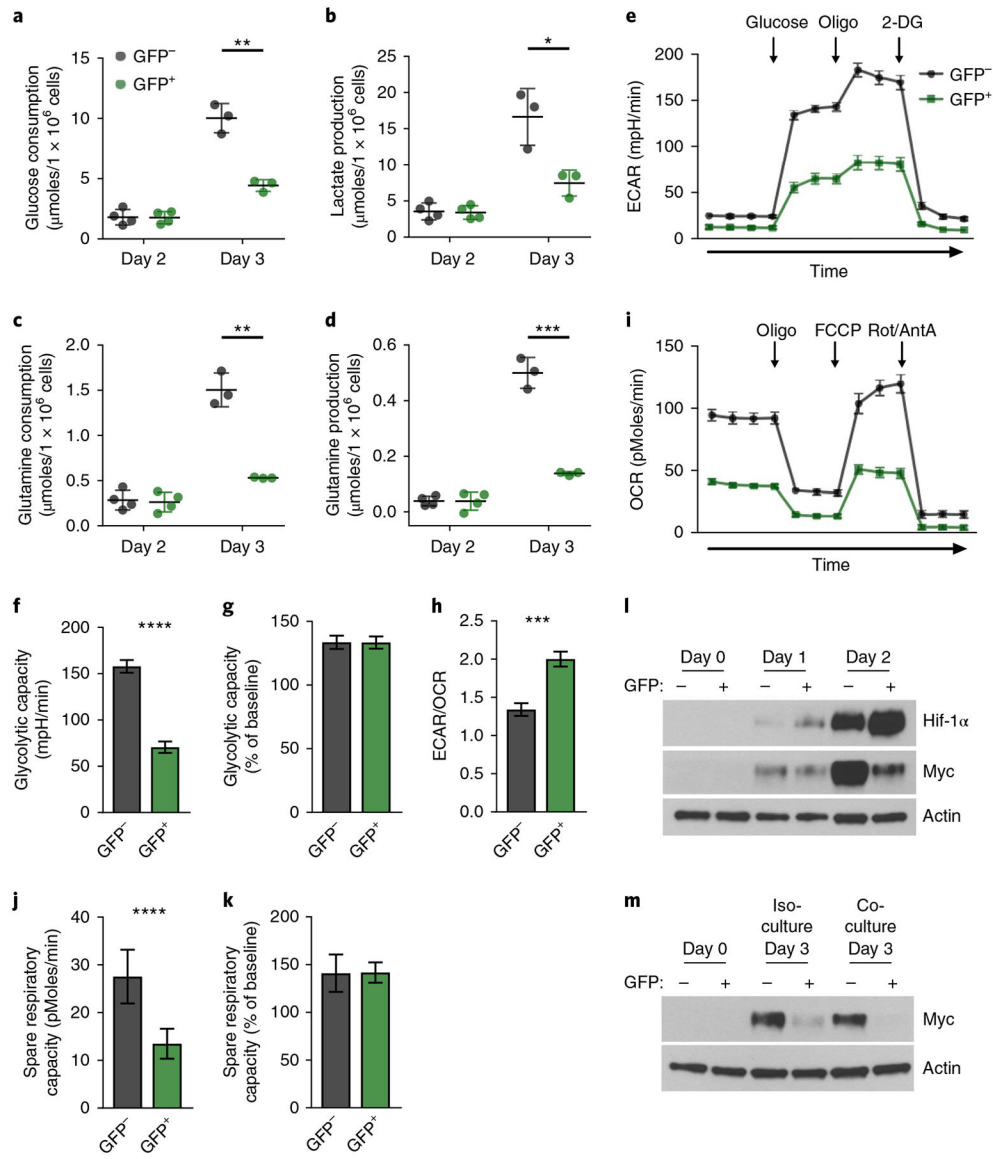


Fig. 3 |. Maintained Foxo1 activity limits CD4 T cell metabolism and results in a failure to sustain Myc expression.

a–d, Growth-medium analysis of glucose consumption (**a**), lactate production (**b**), glutamine consumption (**c**) and glutamate production (**d**) from isocultures on days 2 ($n = 4$) and 3 ($n = 3$). **e–k**, Quantification of ECAR (**e**), glycolytic capacity (**f,g**), OCR (**i**) and spare respiratory capacity (**j,k**) under basal conditions and in response to oligomycin (oligo), fluoro-carbonyl cyanide phenylhydrazine (FCCP), rotenone (Rot)/antimycin A (AntA), glucose and 2-deoxyglucose (2-DG) on day 3 of isocultures. Data are representative of two independent experiments with similar results. ECAR/OCR ratio (**h**) was determined with the glycolytic stress test, for which ECAR traces alone are shown as in **e**. For all graphs, quantification involved a two-tailed Student’s *t* test with no adjustments made for multiple comparisons; center value, mean; error bars, s.d. * $P < 0.05$; ** $P < 0.005$; *** $P < 0.0005$; **** $P < 0.0001$. **l**, Immunoblot analysis of isocultures stimulated with plate-bound anti-CD3 and soluble anti-CD28. Data are representative of three independent experiments with similar results. **m**,

Immunoblot analysis of iso- and cocultures stimulated as in **I**. Data are representative of two independent sorting experiments with similar results. After sorting, a proportion of GFP⁻ and GFP⁺ cells were immediately lysed (Day 0). After 3 d in culture, isolated cultures were lysed and probed, and cocultures were sorted once again for GFP and GFP⁺ populations, lysed and probed. β -actin was used as a loading control.

Author Manuscript

Author Manuscript

Author Manuscript

Author Manuscript

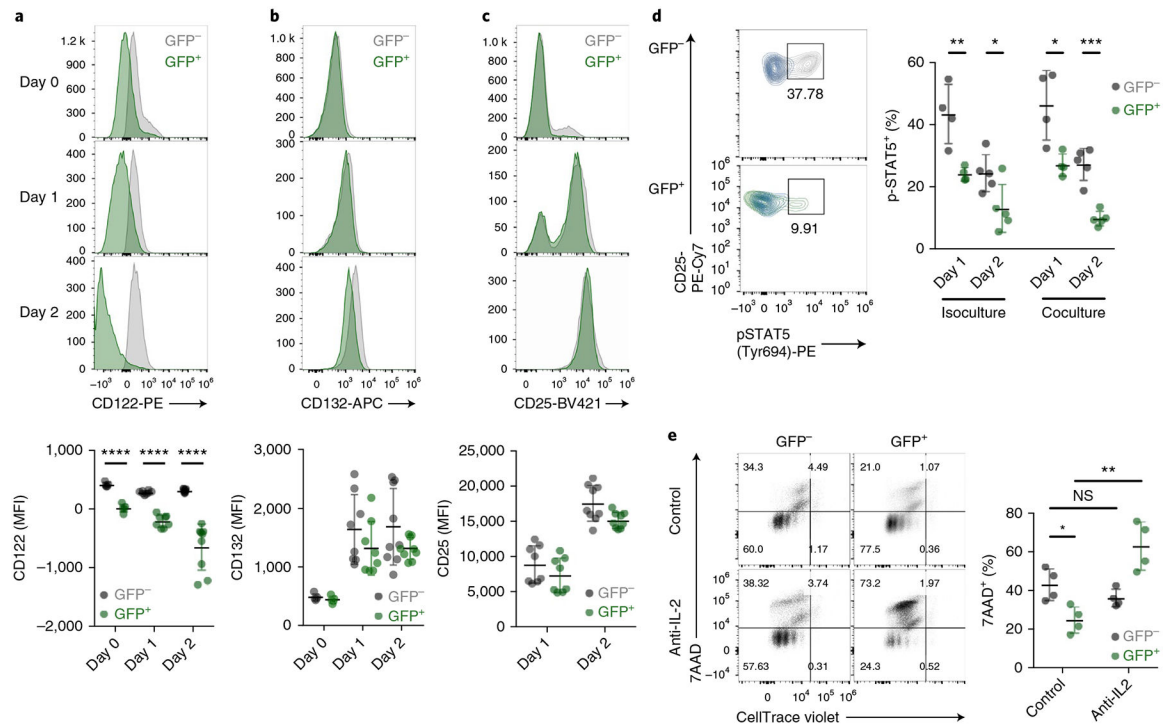


Fig. 4 | Foxo1 mediates downregulation of IL-2R β and decreases STAT5 activation.

a–c, Flow cytometric analysis of GFP and GFP isocultures stimulated for 0, 1 and 2 d with anti-CD3/28 (**a–c**, $n = 7$). MFI, mean fluorescence intensity. **d**, Flow cytometric analysis of GFP $^{-}$ and GFP $^{+}$ iso- and cocultures stimulated for 1 d (representative flow plots shown, isocultures; $n = 4$) and 2 d ($n = 5$) with anti-CD3/28. Blue contours indicate isotype staining. **e**, Isocultures were labeled with CellTrace Violet and stimulated as in **a**, with the additional condition that on day 2, 30 ng/ml anti-IL-2 blocking antibody (diluted in medium) or the equivalent volume of medium alone, was added to isolated cultures, followed by 80 ng/ml anti-IL-2 on day 3. Cells were stained for 7AAD and analyzed by flow cytometry on day 4 ($n = 4$ cultures). Quantification for the proportion of 7AAD $^{+}$ cells on day 4 is shown on the right. For all graphs, quantification involved a two-tailed Student’s t test with no adjustments made for multiple comparisons; center value, mean; error bars, s.d. * $P < 0.05$; ** $P < 0.005$; *** $P < 0.0005$; **** $P < 0.0001$; NS, not significant.

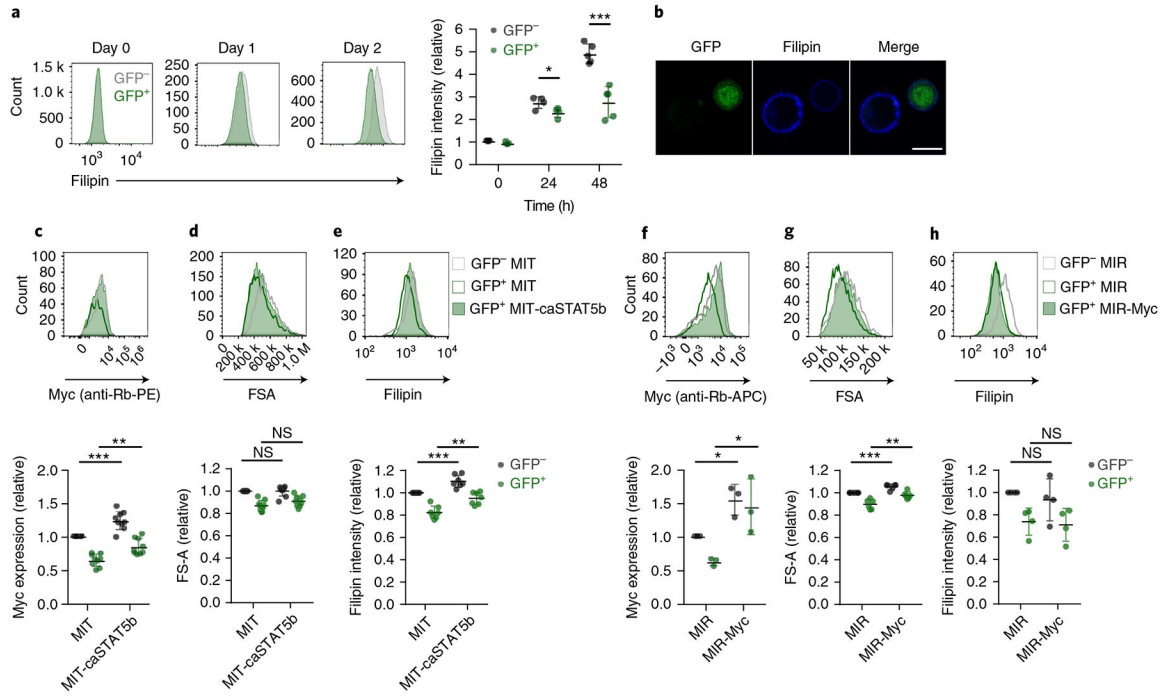


Fig. 5 |. Maintained Foxo1 activity suppresses activation-induced increases in cell size and cholesterol content.

a, Flow cytometric analysis of Filipin staining of isolated cultures stimulated with anti-CD3/28 ($n = 4$). **b**, Representative confocal images of Filipin staining on day 2 of cocultures stimulated as in **a**. Data are representative of three independent experiments with similar results. Scale bar, 10 μ M. **c–e**, Expression of constitutively-active STAT5b (caSTAT5b) in isolated cultures. GFP⁻ and GFP⁺ cells were activated for 24 h before transduction with retrovirus encoding Thy1.1 (MSCV-IRES-Thy1.1; MIT) or Thy1.1 plus caSTAT5b (MIT-caSTAT5b). Flow plots are gated on Thy1.1⁺ transduced cells 48 h post-transduction (**c**, $n = 7$; **d**, $n = 9$; **e**, $n = 7$). **f–h**, Myc overexpression in isolated cultures. GFP⁻ and GFP⁺ cells were activated for 24 h before transduction with retrovirus encoding RFP (MSCV-IRES-RFP; MIR) or RFP plus c-Myc (MIR-Myc). Flow plots are gated on RFP⁺-transduced cells 48 h post-transduction. Analysis of Filipin staining was subsequent to sorting RFP⁺ populations (**f**, $n = 3$; **g**, $n = 6$; **h**, $n = 4$). For all graphs, quantification involved a two-tailed Student's *t* test with no adjustments made for multiple comparisons; center value, mean; error bars, s.d. * $P < 0.05$; ** $P < 0.005$; *** $P < 0.0005$; NS, not significant.

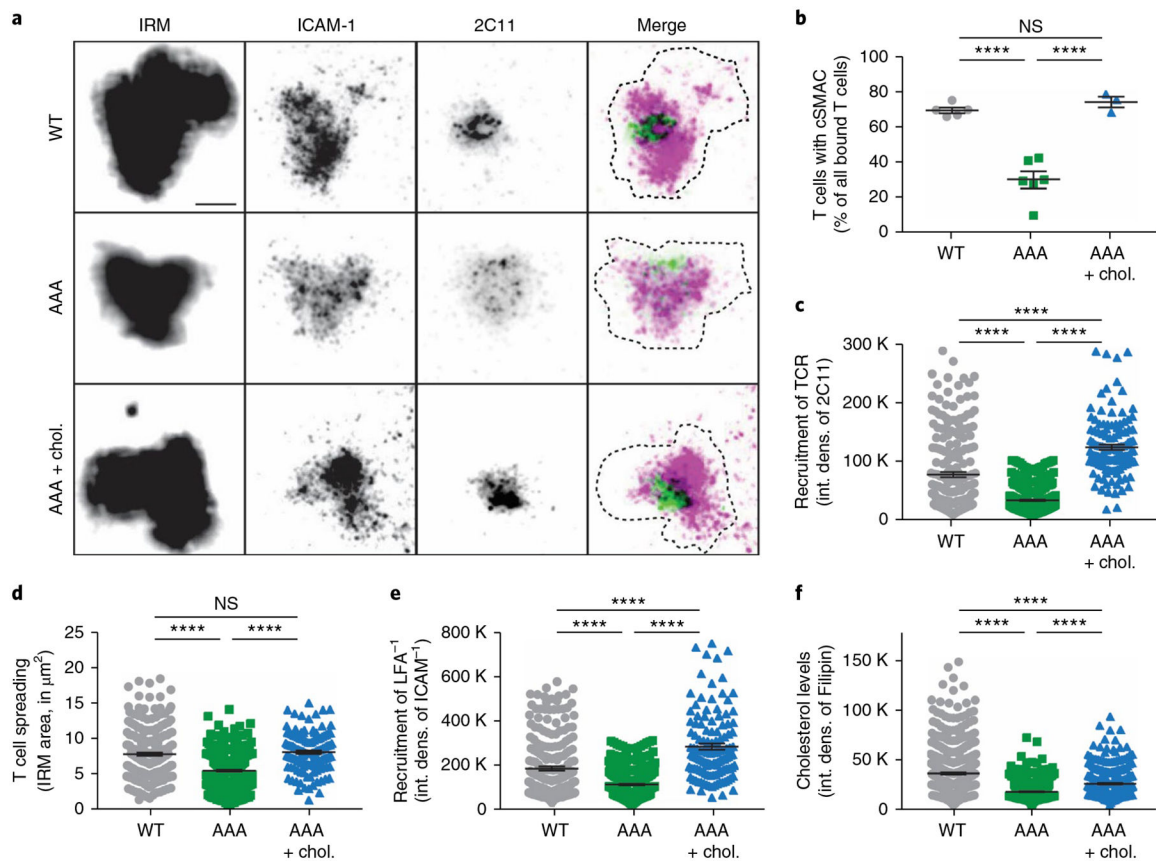


Fig. 6 | Cholesterol-dependent immunological synapse formation is disrupted by maintained Foxo1 activity.

a, Representative total internal reflection fluorescence microscope images of mouse CD4 T cells expressing wild-type or constitutively active Foxo1 with or without water-soluble cholesterol supplementation, interacting with SLBs containing fluorescent ICAM-1 and CD80, and anti-TCR 2C11. SLB-bound T cell surface was visualized by interference reflection microscopy (IRM). Data are representative of three independent experiments with similar results. Scale bar, 5 μm . **b**, Quantification of immunological synapse formation by T cells, as a percentage of all SLB-bound T cells per experiment. Successful formation was defined by the appearance of a highly dense 2C11 area excluding ICAM-1 at the site of SLB interaction (wild type, $n = 6$ cultures; AAA, $n = 6$; AAA + cholesterol (chol.), $n = 3$). **c–e**, Quantification of TCR and LFA-1 recruitment, as determined by integrated density (int. dens.) of 2C11 and ICAM-1, respectively. IRM was used to determine T cell spreading, and area was used as a mask for quantification of integrated fluorescence density. K denotes thousands. **f**, Cellular levels of cholesterol, determined by Filipin staining. Graphs indicate percentage or mean \pm s.e.m. One-way analysis of variance was performed on all datasets and indicated $P < 0.0001$ for each. P values were determined with the Mann–Whitney two-tailed t test to directly compare two individual groups. **** $P < 0.0001$; NS, not significant.

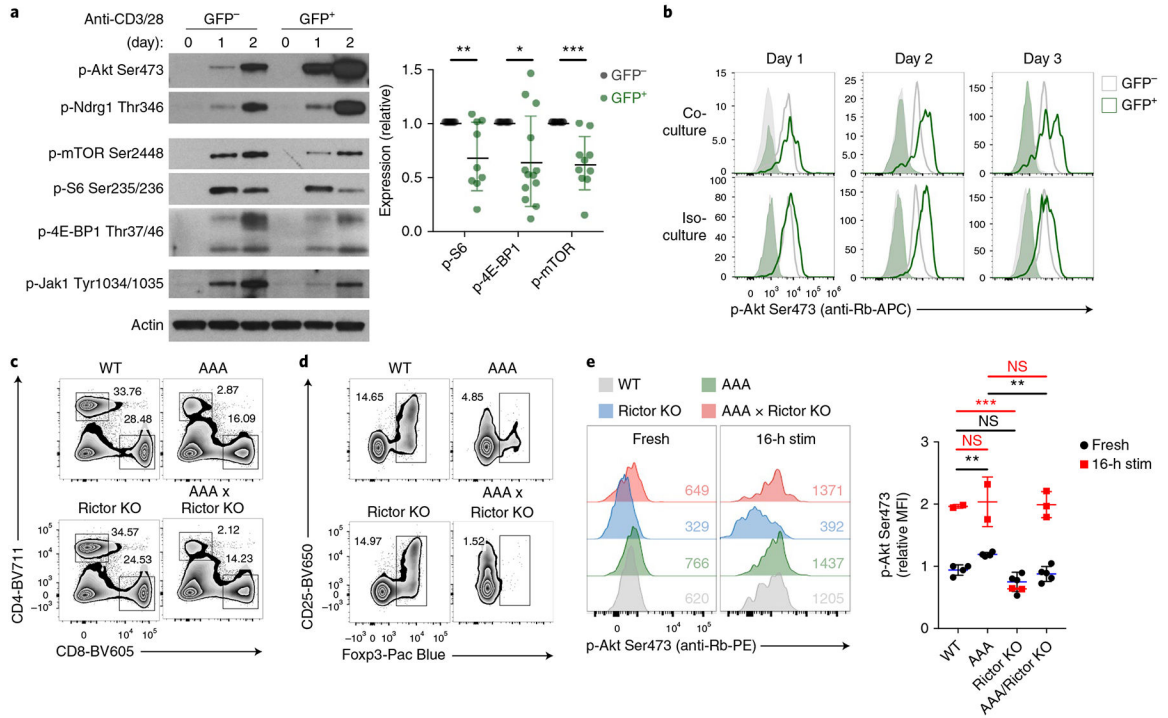


Fig. 7 | Foxo1 activity simultaneously increases Akt and suppresses mTORC1 activation.
a, Immunoblot analysis of isocultures stimulated for 1 or 2 d with plate-bound anti-CD3 and soluble anti-CD28. After sorting, a proportion of GFP⁻ and GFP⁺ cells were immediately lysed (day 0). Quantification is for expression on day 2 (normalized to β-actin; p-S6, *n* = 9 cultures; p-4E-BP1, *n* = 13, p-mTOR, *n* = 10). **b**, Flow cytometric analysis of p-Akt Ser473 staining on iso- and cocultures on days 1, 2 and 3 post-activation with plate-bound anti-CD3 and soluble anti-CD28. Open histograms are GFP⁻ and GFP⁺ populations as indicated; lightly shaded histograms show isotype-control staining for each population. Data are representative of three independent experiments with similar results. **c**, Flow cytometric analysis of splenocytes from 8-week-old CD4^{Cre} (WT), CD4^{Cre} Foxo1^{AAA/+} (AAA), CD4^{Cre} Rictor^{fl/fl} (Rictor KO) and CD4^{Cre} Rictor^{fl/fl} Foxo1^{AAA/+} (AAA × Rictor KO) littermates. Data are representative of similar results for *n* = 4 mice. **d**, Flow cytometric analysis of CD4⁺ T cells from the same mice as in **c**. **e**, Flow cytometric analysis of p-Akt Ser473 measured in CD4⁺ T cells directly ex vivo (fresh; *n* = 4 mice for all except AAA × Rictor KO, where *n* = 5), and after 16 h in culture with plate-bound anti-CD3 and soluble anti-CD28 (16-h stimulation (stim); *n* = 2, except for AAA × Rictor KO, *n* = 3). For all graphs, quantification involved a two-tailed Student's *t* test with no adjustments made for multiple comparisons; center value, mean; error bars, s.d. **P* < 0.05; ***P* < 0.005; ****P* < 0.0005; NS, not significant.

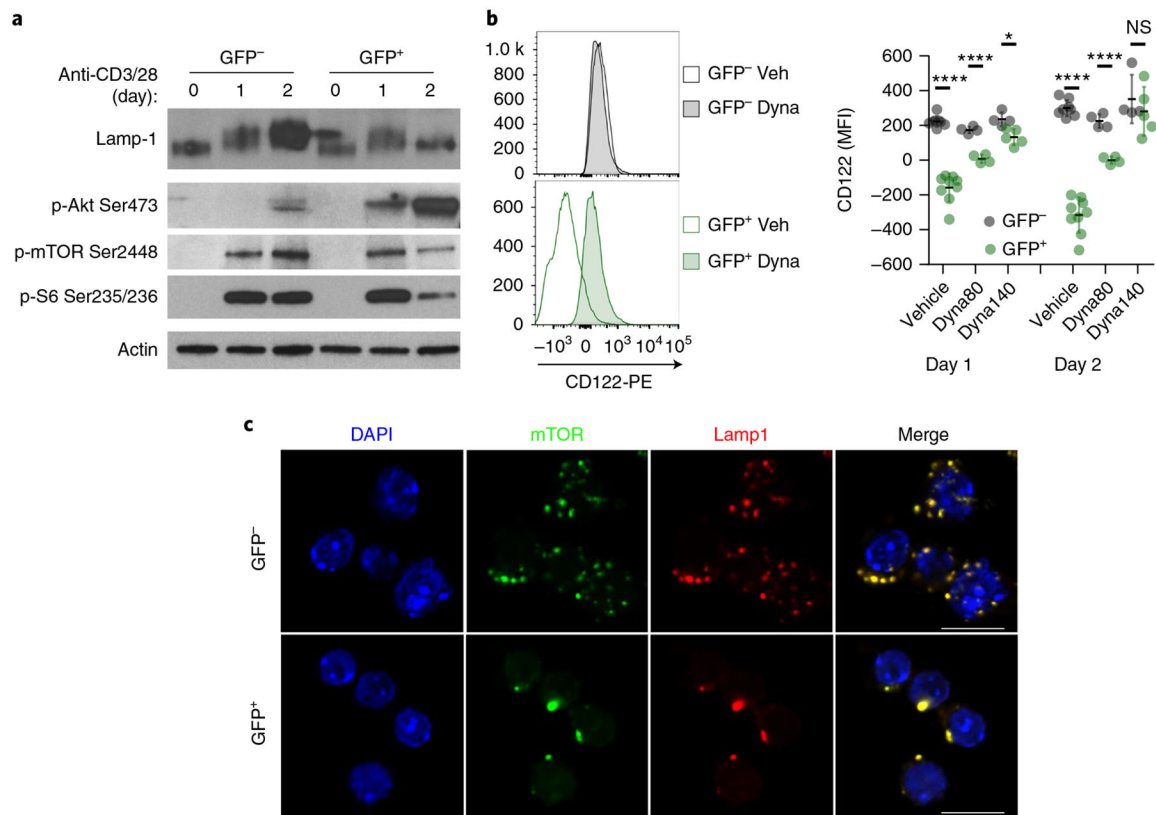


Fig. 8 |. Impaired lysosomal biogenesis and endocytosis of IL-2R β upon maintaining Foxo1 activity.

a, Immunoblot analysis of isocultures stimulated for 1 or 2 d with plate-bound anti-CD3 and soluble anti-CD28. After sorting, a proportion of GFP⁻ and GFP⁺ cells were immediately lysed (day 0). Data are representative of four independent experiments with similar results. β -actin was used as a loading control. **b**, Flow cytometric analysis and quantification of isocultures stimulated for 1 or 2 d with plate-bound anti-CD3 and soluble anti-CD28 with vehicle (Veh) or Dynasore (Dyna; 80 and 140 mM, Dyna80 and Dyna140, respectively; $n = 5$). Representative plots are of day 1 post-activation with 140 mM Dynasore. Quantification involved a two-tailed Student's t -test with no adjustments made for multiple comparisons; center value, mean; error bars, s.d. * $P < 0.05$; **** $P < 0.0005$; NS, not significant. **c**, Representative immunofluorescence images of mTOR ($n = 3$ independent experiments with similar results), Lamp-1 and DAPI nuclear staining on day 2 of isocultures stimulated as in **a**. Scale bar, 10 μ M.